Mapping geomagnetic secular variation at the core-mantle boundary

Geophysical Journal International

Geophys. J. Int. (2011) **186,** 521–528 doi: 10.1111/j.1365-246X.2011.05066.x

Mapping geomagnetic secular variation at the core–mantle boundary

R. Holme,[1] N. Olsen[2] and F. L. Bairstow[1]*

[1]*School of Environmental Sciences, University of Liverpool,* L69 3GP, *UK. E-mail: holme@liv.ac.uk*
[2]*DTU Space, Juliane Maries Vej* 30, 2100 *Copenhagen, Denmark*

Accepted 2011 April 28. Received 2011 April 11; in original form 2011 January 26

SUMMARY

Data from recent satellite missions have vastly increased the resolution of models of the geomagnetic field, and its first and second time derivatives – secular variation (SV) and secular acceleration (SA). The spectra of both SV and SA are 'blue' at the core–mantle boundary, both well-fit by functions proportional to $l(l+1)$ where l is the spherical harmonic degree. The ratio of the two spectra defines a timescale for geomagnetic variations of approximately 10 yrs for all resolvable harmonic degrees. The blue spectra should prevent meaningful maps of the SV being generated; nevertheless, the coherence of the maps up to harmonic degree 13 suggests that it is possible to obtain useful insight from their examination. Low SV is confirmed under the Pacific, but also revealed under the North Atlantic and Antarctica. These features are more readily explained in terms of dynamo control through thermal core–mantle coupling than by electromagnetic screening. Comparison with maps from measurements prior to the recent satellites, using the 'Comprehensive Model', suggests that models back to at least 1970 are sufficiently good to enable direct comparison of the SV.

Key words: Magnetic field; Rapid time variations; Satellite magnetics.

1 INTRODUCTION

The geomagnetic field is a sensitive probe of the structure and dynamics of the Earth, particularly the deep Earth. It shows significant variations down to decadal timescales and shorter, much shorter than most processes involving the Earth's interior geodynamics. These changes, defined in terms of magnetic secular variation (SV), the first time derivative of the field, have been used to study core–mantle interactions, and to constrain flow in the core and the dynamo process responsible for generating the field. The detail with which the SV can be modelled has been substantially improved by two recent satellite missions: Ørsted, launched in 1999 February (Neubert *et al.* 2001) and still in orbit at time of writing, and CHAMP (Reigber *et al.* 2002), which flew between 2000 July and 2010 September. Both were polar, low-Earth orbiting satellites, providing broadly continuous globally distributed vector magnetic measurements throughout their missions. These data have yielded very accurate time-dependent models of the magnetic field, for example, the GRIMM series (Lesur *et al.* 2008, 2010), the POMME series (e.g. Maus *et al.* 2006), and the CHAOS series (Olsen *et al.* 2006, 2009, 2010b). The data and models have been applied towards understanding of core processes, for example, to attempt high-resolution models of the flow at the surface of the core (e.g. Hulot *et al.* 2002; Holme & Olsen 2006; Gillet *et al.* 2009). However, direct analysis of the SV itself has been limited, because the spectrum of the SV at the core–mantle boundary (CMB) is 'blue', meaning that its power increases with spherical harmonic degree (Holme & Olsen 2006). As a result, mapping of the SV must be suspect, because the power in the higher degree harmonics, not yet resolvable by the data, most likely exceeds the power of the parts of the field which can be resolved.

However, that a process is mathematically poorly posed, or even formally impossible, is rarely a hindrance in studies of deep-Earth geophysics! In this paper, we examine whether SV maps can be informative, even if they are not converged. We use the most recent CHAOS model designated CHAOS-4. We first consider the resolution of the SV in the CHAOS model by examining its spectrum. We then use simple truncation to examine the content of the SV at different length scales, and, surprisingly, find considerable coherence as harmonic degree is increased. By comparing with the Comprehensive Model over earlier periods, we suggest that SV maps may be usefully interpreted prior to the satellite era. Finally, we discuss what geophysical insight we may obtain from our study.

2 THE SECULAR VARIATION POWER SPECTRUM

The magnetic field $\mathbf{B}$ is represented as the gradient of a scalar potential Φ satisfying Laplace's equation, so that $\mathbf{B} = -\nabla\Phi$ and $\nabla^2\Phi = 0$. In spherical geometry, the solution to this equation is

*Now at: PGS Exploration (UK) Ltd, Weybridge, Surrey, KT13 0NY, UK.

conveniently expressed in terms of spherical harmonics

$$\Phi = a \sum_{l=1}^{\infty} \left(\frac{a}{r}\right)^{l+1} \sum_{m=0}^{l} P_l^m \left(\cos\theta\right)\left(g_l^m \cos m\phi + h_l^m \sin m\phi\right). \quad (1)$$

Here, (r, θ, ϕ) are spherical coordinates given by distance from the centre of the Earth, colatitude and longitude, a is the radius of the Earth (taken as 6371.2 km), and P_l^m are Schmidt semi-normalized associated Legendre functions in $\cos\theta$, of degree l and order m. $\{g_l^m, h_l^m\}$ are the set of time-dependent Gauss coefficients which parameterize the field, from which it is possible to define coefficients for the SV $\{\dot{g}_l^m, \dot{h}_l^m\}$ and secular acceleration (SA) $\{\ddot{g}_l^m, \ddot{h}_l^m\}$, where the dots denote time derivatives.

In this paper, we consider the CHAOS-4 model (Olsen *et al.* 2010a). This is an extension of the CHAOS-3 model (Olsen *et al.* 2010b); the methodology follows that model but with an additional year of model and data coverage. Other developments include regularization of $|d^3 B_r/dt^3|$, and of $d^2 B_r/dt^2$ at the endpoints (rather than the magnitude of **B** as for CHAOS-3), and CHAMP data used for all nighttimes, but only with electron density $N_e < 10^{-5}\,\mathrm{cm}^{-3}$ to avoid contamination from plasma bubbles. Time dependence in CHAOS-4 is modelled up to degree and order 20 on a basis of order 6 B-splines, allowing straightforward calculation of time derivatives. Further details and model coefficients are provided at http://spacecenter.dk/files/magnetic-models/CHAOS-4.

Various authors (e.g. Mauersberger 1956; Lowes 1966) noted independently that the mean square value of the field, integrated over a spherical surface, has a simple form

$$\frac{1}{A}\oint \mathbf{B}\cdot\mathbf{B}\,dA = \sum_{l=1}^{\infty}(l+1)\left(\frac{a}{r}\right)^{2l+4}\sum_{m=0}^{l}\left(\left(g_l^m\right)^2 + \left(h_l^m\right)^2\right), \quad (2)$$

where A is the area of the sphere at radius r. It has proved instructive for a given radius r to plot the individual contributions to this integral from components of different degree l (effectively wavenumber) against that degree, giving a 'power spectrum' of the field

$$W(l, r) = (l+1)\left(\frac{a}{r}\right)^{2l+4}\sum_{m=0}^{l}\left(\left(g_l^m\right)^2 + \left(h_l^m\right)^2\right). \quad (3)$$

It has been recognized for many years (e.g. Lowes 1974; Langel & Estes 1982) that this spectrum is approximately 'white' for degrees 1–13 when plotted at c, the core radius. McLeod (1996) demonstrated that $W(l, c)(2l + 1) \approx$ constant fits the observed spectrum well for degrees above 2, so

$$W(l, c) \propto \frac{1}{2l+1} \quad (4)$$

[Voorhies *et al.* (2002) present alternative algebraic relations which give essentially the same behaviour.]

The idea of a spectrum has been generalized to define a similar expression for the mean-square SV (e.g. Hulot & Le Mouël 1994; Voorhies 2004; Holme & Olsen 2006; Gillet *et al.* 2010), plotting

$$W'(l, r) = (l+1)\left(\frac{a}{r}\right)^{2l+4}\sum_{m=0}^{l}\left(\left(\dot{g}_l^m\right)^2 + \left(\dot{h}_l^m\right)^2\right) \quad (5)$$

against l. The ratios of the individual terms of the SV spectrum to the corresponding main field spectral terms define timescales for different degrees of the field, independent of radius r

$$\tau_l = \sqrt{\frac{W(l, r)}{W'(l, r)}} = \sqrt{\frac{\sum_{m=0}^{l}\left(\left(g_l^m\right)^2 + \left(h_l^m\right)^2\right)}{\sum_{m=0}^{l}\left(\left(\dot{g}_l^m\right)^2 + \left(\dot{h}_l^m\right)^2\right)}} \quad (6)$$

(Stacey 1992, p. 355), which may be regarded as correlation times (Hulot & Le Mouël 1994). Some dynamo simulations (e.g. Christensen & Tilgner 2004) yield a relation for these constants of the form

$$\tau_l \propto \frac{1}{l}. \quad (7)$$

Examining a range of field models from both satellite and historical data, Lhuillier *et al.* (2011) were unable to reject the hypothesis that this relation also provided a good fit for observational estimates of the timescales (at least for degrees of 3 and above); given eq. (4), this requires for the SV spectrum that

$$W'(l, c) \propto l + \frac{1}{2} \quad (8)$$

(or some other function roughly proportional to the spherical harmonic degree). In contrast, McLeod (1996) proposed a SV spectrum of the form

$$W'(l, c) \propto l\left(l + \frac{1}{2}\right)(l+1), \quad (9)$$

which Voorhies (2004) derives on the assumption of narrow-scale surface core flow; he also proposes an alternative relation

$$W'(l, c) \propto l(l+1), \quad (10)$$

which he argues would result if SV is generated by partially resolved eddies in the flow, or as a result of electromagnetic smoothing due to lateral heterogeneity of electrical conductivity in the deep mantle. (The derivation is given in Voorhies (1998).) An alternative formulation $W'(l, c) \propto (2l + 1)^2$ is observationally indistinguishable from eq. (10); this could be attractive as each harmonic degree has $2l + 1$ degrees of freedom.

We test these predictions against the SV spectra at the CMB for the CHAOS-4 model at epochs 2002.0, 2005.0 and 2008.0, choosing times away from the ends of the model to avoid the risk of modelling end effects. In Fig. 1, we follow McLeod (1996) plotting the spectra at the CMB ($r = c = 3485$ km) divided by the algebraic functions given in eqs (8)–(10). If the function correctly fits the observed spectrum, these plots should yield horizontal straight lines. This

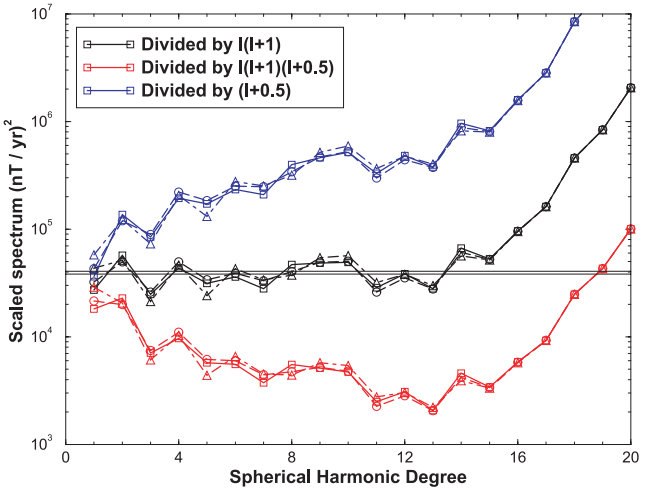

Figure 1. Comparison of different algebraic relations for SV spectrum at the CMB, $r = c$. Blue lines correspond to eq. (8), red lines to eq. (9) and black lines to eq. (10). Solid lines are for 2002, dashed lines for 2005 and dot-dashed lines for 2008. The closer to a horizontal line, the better the chosen function represents the spectrum. Thin horizontal lines give the range of estimates of the constant of proportionality from eq. (11).

is best achieved by eq. (10) at least up to degree 12 or 13, above which observational uncertainties start to be influential; thus we will assume that the SV spectrum obeys

$$W'(l, c) = ql(l + 1). \tag{11}$$

The consequence of this functional form is a relation for the timescale from eq. (6) of

$$\tau_l \propto \frac{1}{\sqrt{l(l + 1)(2l + 1)}} \tag{12}$$

so approximately proportional to $l^{-3/2}$. This relation is in close agreement with the earlier estimate of $l^{-1.45}$ for the CO2003 model that Holme & Olsen (2006) obtained from a power-law fit, but disagrees with the suggestion of Lhuillier *et al.* (2011) of l^{-1} motivated by results from dynamo theory (which would correspond to the upper, blue, lines in Fig. 1).

To estimate q, and to put statistical bounds on the fit, we follow Hulot & Le Mouël (1994), and assume that each SV Gauss coefficient is normally distributed with zero mean and some standard deviation $\sigma(l)$ which is a function of the wavenumber. (Note that the assumption of zero mean fails, at least for the axial dipole SV $\dot{g}_1^0$ for which the steady decay of the dipole over historical time gives a mean of approximately 15 nT yr^{-1}. However, the axial dipole SV is substantially smaller than that of the equatorial dipole, as a result of which this failure does not strongly influence the following results.) From this it follows that the variable $(\dot{g}_l^m/\sigma(l))^2$ is χ^2-distributed with one degree of freedom. Hence the power $W'(l, c)$ is also χ^2-distributed; with appropriate choice of $\sigma(l)$ we define the mean $\mu = ql(l + 1)$, with corresponding standard deviation $\sqrt{\frac{2}{2l+1}}\mu$. The best fit value of q, assuming that observational error on the Gauss coefficients and so on their power is negligible, is obtained by the weighted mean of $W'(l, c)/(l(l + 1))$ (in effect giving equal weight to every Gauss coefficient). A less rigorous, but perhaps more conservative and reasonable, estimate might also be to take a simple mean of $W'(l, c)/(l(l + 1))$, allowing for the fact that due to downward continuation the uncertainties increase with degree. We obtain estimates of q for $l = 1$ to 12, to avoid possible contamination from noise. The thin horizontal lines plotted in Fig. 1 give the range of values obtained for the three epochs using both methods; as can be seen, there is little difference between them (the values of q vary between 38 000 and 40 000). The low degree spectrum has often previously been fit by a power law seeking amplitude and source depth; we prefer the relation (11) because it is theoretically motivated, and also requires a fit of only one free parameter rather than two (with the source depth defined physically as the CMB).

Taking $q = 38\,000$, Fig. 2 compares eq. (11) against the CHAOS-4 SV spectra at the CMB at epochs 2002.0, 2005.0 and 2008.0, along with 1σ error bounds given by $W'(l, c)(1 \pm \sqrt{2/(2l + 1)})$. The curves for each of the three epochs fit appropriately closely in relation to the error bounds, providing strong support for the appropriateness of the fit and the underlying statistical assumptions. A clear break in slope of the spectrum is seen at degree $l \approx 14$. Above this, the spectrum is dominated by the effects of measurement and modelling uncertainty; this is well-characterized by an exponential fit to degrees 16 and above (the red line). This simple model of the combination of two sources (the dashed blue line) provides an excellent fit to the CHAOS-4 model spectra, far better than can be obtained for a model of the spectrum of the field itself. This suggests an origin for the SV at small scales, as there is no evidence in the spectrum for influence from different strength field harmonics (e.g. strong dipole and weak quadrupole), which would

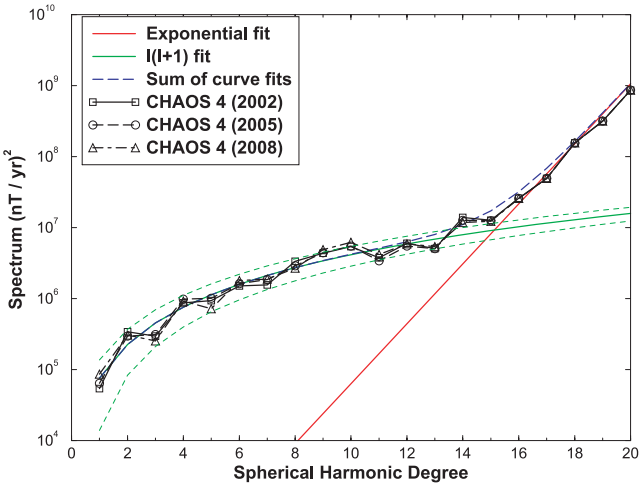

Figure 2. Spectra of the CHAOS-4 SV at the CMB, $r = c$. Green line gives theoretical model, dashed lines approximate 1σ error bounds.

give rise to much larger deviations from the general relation for the spectrum. If, for example, SV was generated primarily by diffusion, we would expect the structure of the SV spectrum to match that of the main field, and hence with a lower power at $l = 2$. More detailed spectral structure can also be seen (which in itself calls into question the model of the Gauss coefficients as statistically independent random variables); powers at even degrees fall above the trend line, while odd degrees fall below it (previously reported by Holme & Olsen 2006). Simple interpretations, such as a difference in power between either equatorially symmetric ($l + m$ even) or antisymmetric ($l + m$ odd) terms, or of azimuthally symmetric (m even) rather than antisymmetric (m odd) terms, are not borne out by detailed examination. We return to this point later.

We further extend the use of spectra to define a SA spectrum,

$$W''(l, r) = (l + 1)\left(\frac{a}{r}\right)^{2l+4} \sum_{m=0}^{l} \left(\left(\ddot{g}_l^m\right)^2 + \left(\ddot{h}_l^m\right)^2\right). \tag{13}$$

In Fig. 3, we plot $W''(l, c)$, the SA spectrum at the CMB. Motivated by the success of the fit to the SV spectrum, we again plot a trend curve given by eq. (11), again with statistically derived 1σ error bounds. There is some difference in level of the SA spectra

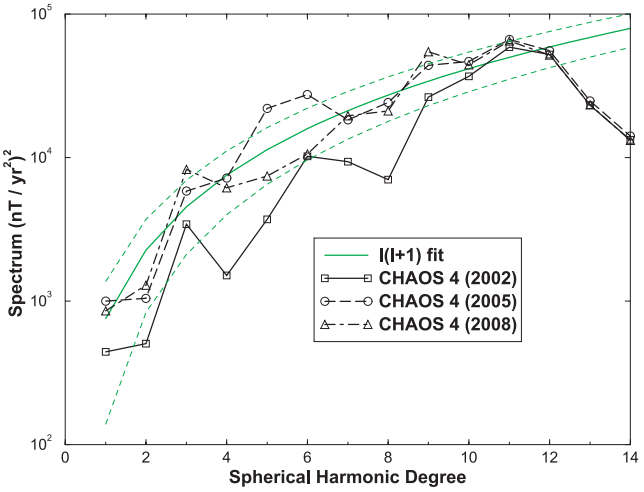

Figure 3. Spectra of the CHAOS-4 SA at the CMB, $r = c$. Green line gives theoretical model, dashed lines approximate 1σ error bounds.

between epochs, possibly due to end-effects from the spline model, but also likely to result from physical processes—so-called Geomagnetic jerks (Mandea *et al.* 2010). All spectra drop rapidly after degree 12, due to damping in the model construction. However, for degrees up to 12 in the middle of the modelling interval, the fit of the trend curve to spectra from 2005 and 2008 is striking, again in good agreement within the error bounds, particularly as SA models are less well constrained than their SV counterparts (there is considerably more variation between different models, and the fine details are a sensitive function of modelling strategy).

We follow Lesur *et al.* (2008) in using the spectra of SV and SA to define a further geomagnetic timescale

$$\tau'_l = \sqrt{\frac{\sum_{m=0}^{l}\left(\left(\dot{g}_l^m\right)^2 + \left(\dot{h}_l^m\right)^2\right)}{\sum_{m=0}^{l}\left(\left(\ddot{g}_l^m\right)^2 + \left(\ddot{h}_l^m\right)^2\right)}}. \tag{14}$$

Because both SV and SA are fit by the same trend function (11), the time constants τ'_l are approximately the same for all degrees, equal to about 10 yrs. Lesur *et al.* (2008), working with the GRIMM model, did not find that τ'_l was independent of degree, but the more recent GRIMM-2 model (Lesur *et al.* 2010) does show a timescale independent of degree, in agreement with our results (V. Lesur, personal communication, 2011). The common power spectral structure and consequent uniform decadal time scale is clearly worthy of further attention. (Note that the 10-year timescale is also the approximate length of available satellite data and the CHAOS-4 model; however, see Section 4 below.)

3 PLOTTING THE TRUNCATED SECULAR VARIATION

The spectra of both SV and SA are 'blue': their power increases with spherical harmonic degree. This can be quantified using eq. (11): the cumulative power to degree l is

$$\frac{q}{3}l(l+1)(l+2) \tag{15}$$

so the ratio of the power in the first neglected degree $(l+1)$ to the power in all lower degrees is $3/l$; thus, power at degree 13 is equal to 25 per cent of the power in all degrees 1–12. We would therefore expect the power of the missing components to exceed those which are observable, rendering mapping of the SV impossible. Nevertheless, we consider here maps of the SV plotted at the CMB for different truncation levels. For epoch 2005.0 (approximately the midpoint of the CHAOS-4 model), the models of the SV of the radial magnetic field component $\dot{B}_r$ are plotted in Fig. 4 scaled to their maximum magnitude in each case. For clarity, the zero contour is not plotted. It is striking that there is a strong visual coherence between the maps as the higher-degree components of the SV are added. The plots start to become noisy from degree 14, as would be expected from the spectrum (Fig. 2), but even at degree 16, the strong features in the SV (particularly in the Atlantic hemisphere) are still clearly visible; this clarity is not overwhelmed by the noise until degree 19

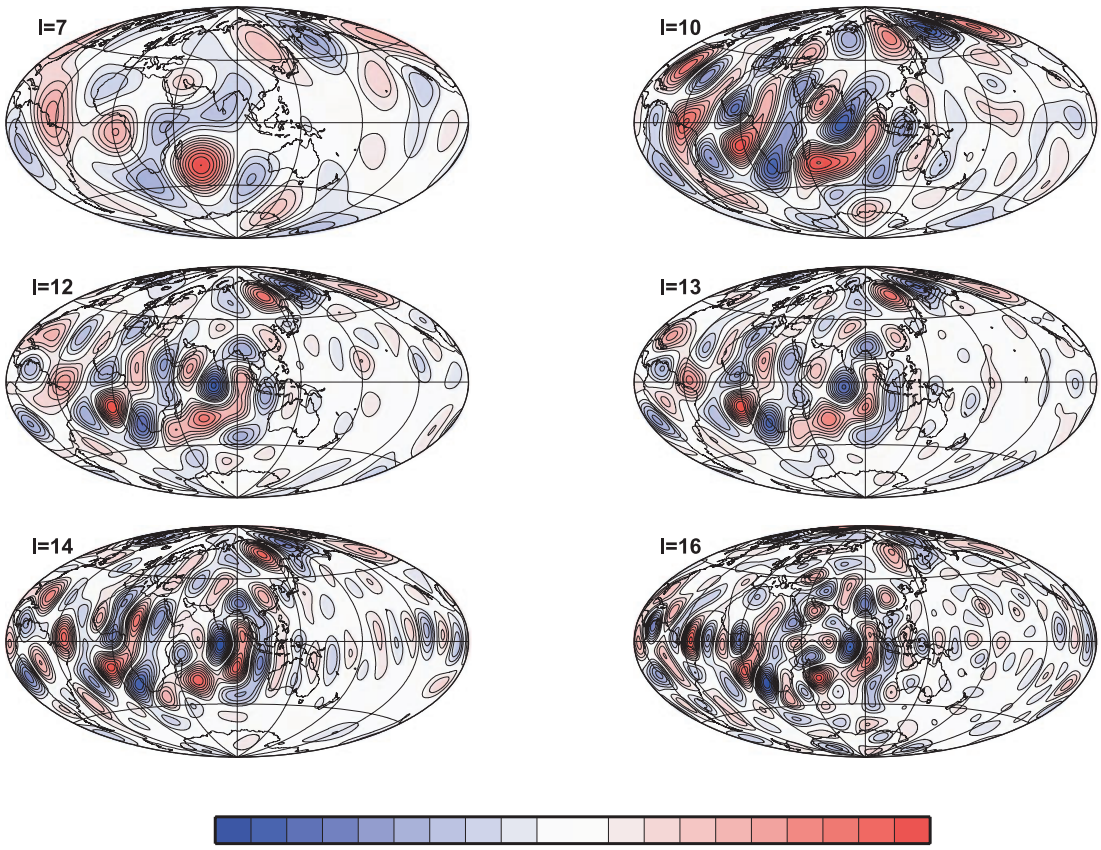

Figure 4. Plots of the radial component of the secular variation at the CMB, truncated to spherical harmonic degrees (7,10,12,13,14,16). Scale bar defined by the maximum magnitude (positive or negative) for each plot. For clarity, the zero contour is not plotted. Position of the continents plotted to provide a reference frame.

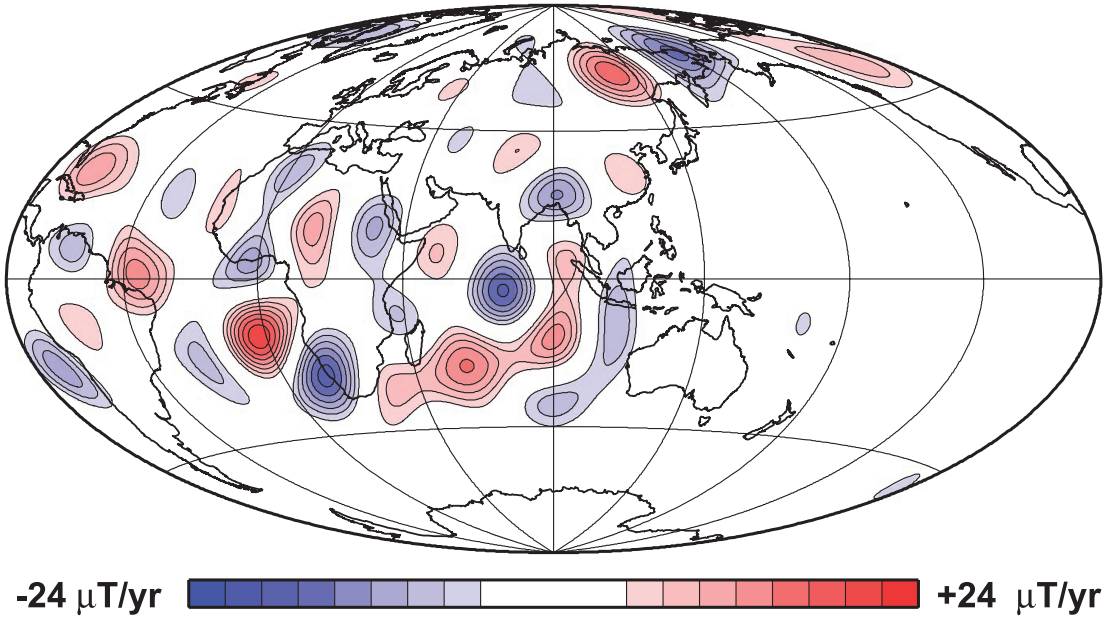

Figure 5. Radial component of CMB secular variation for CHAOS-4, 2005.0, truncated to spherical harmonic degree 13, plotting only the stronger features of the SV.

or 20. The 'optimal' truncation for plotting is to degree 13, as would be expected from the spectrum (Fig. 2). Formal justification of this is difficult: for example, standard expressions for correlation can be written in terms of spectral expansions, so by definition adding any higher spherical harmonic degree will worsen the correlation. Higher resolution may be possible at low latitudes, as the 'noise' in the measurements is dominated by high-latitude magnetic fields, but choosing truncation at $l = 13$ should allow maps with uniformly low noise contamination at all locations. SV is low under the Pacific, as would be expected from previous studies, but considering the degree 13 map, it is equally low under Antarctica and the North Atlantic. The low SV under the Pacific and North Atlantic can also be seen in previous maps (e.g. Lesur *et al.* 2008, 2010; Olsen *et al.* 2009), but the colour scheme here brings the regions out more clearly; in the earlier models, low SV under Antarctica is obscured by noise. Olsen *et al.* (2009) attempted to limit noise contamination by tapering the SV [using formalism given by Wardinski & Holme (2006)]; however, while this may result in a realistic spectrum for the SV, even when tapered the higher harmonics (degree 15 and above) will still be dominated by the contribution from the noise.

Overall, the visual coherence of the different maps suggests that, instead of higher-degree structure 'swamping' weaker, lower-degree, structure, adding higher-degree SV sharpens features that are already present. This observation suggests that non-minimum-norm methods, for example, maximum entropy methods (e.g. Jackson 2003; Gillet *et al.* 2007), which do not penalize sharp peaks, may be appropriate for modelling the SV in future. Overall, it is plausible that the map truncated to degree 13 may give a fair representation of the large-scale structure of the SV at the CMB. To consider this further, we present in Fig. 5 a map of the SV to degree 13, but plotted so that SV less than 20 per cent of maximum (and the contours corresponding to this SV) is not plotted. By doing so, we remove weak features in the SV which may draw the eye, and concentrate solely on the strong, and therefore robust, features. With this colour scale, the strong features of the SV are even more evident: some strong SV foci located under eastern Siberia, and particularly clear equatorial patches in the Atlantic hemisphere, associated with westward drifting magnetic flux patches in that region. The Atlantic features are to be expected, but also are of additional interest. The patches are approximately of azimuthal wavenumber 8 (order 8 harmonics), with a general form of north–south pairs of opposite sign, although lacking strong equatorial antisymmetry. The canonical spherical harmonic with this structure corresponds to the Gauss coefficient h_9^8, although this additionally displays the perfect equatorial antisymmetry not present in the SV map. However, the patches are limited to longitudes approximately $-90^\circ < \phi < 90^\circ$. We filter the harmonic corresponding to h_9^8, multiplying it by a function that has value one for $-90^\circ < \phi < 90^\circ$, and zero in the other hemisphere. We then expand this spectrally, truncating at spherical harmonic degree 20. The result is plotted in Fig. 6(a); in Fig. 6(b), we plot the corresponding power spectrum for this synthetic field. The central peak at the wavenumber of the original harmonic (degree 9) is clear, but the windowing of the field also provides power at even wavenumbers. The observed spectrum of the SV (Fig. 2) expresses this structure: even degree power is amplified, and odd degree lowered, with the exception of a peak at degree 9. We thus suggest that the fine structure of the SV spectrum noted above arises from the dominance of this equatorial part of the SV under the Atlantic.

4 COMPARISON WITH OTHER MODELS—THE COMPREHENSIVE MODEL

It is interesting to compare the results for the the CHAOS-4 model with other models covering the period of the last decade, and with models for earlier times. Spectra are presented in Fig. 7. Of models derived from recent satellite data, we show two precursors of CHAOS-4, the CHAOS-3 model (Olsen *et al.* 2010b), and an earlier model, CO2003 (Holme & Olsen 2006), and from another modelling group, the GRIMM-2 model (Lesur *et al.* 2010). From earlier data, we show two epochs of the Comprehensive model of

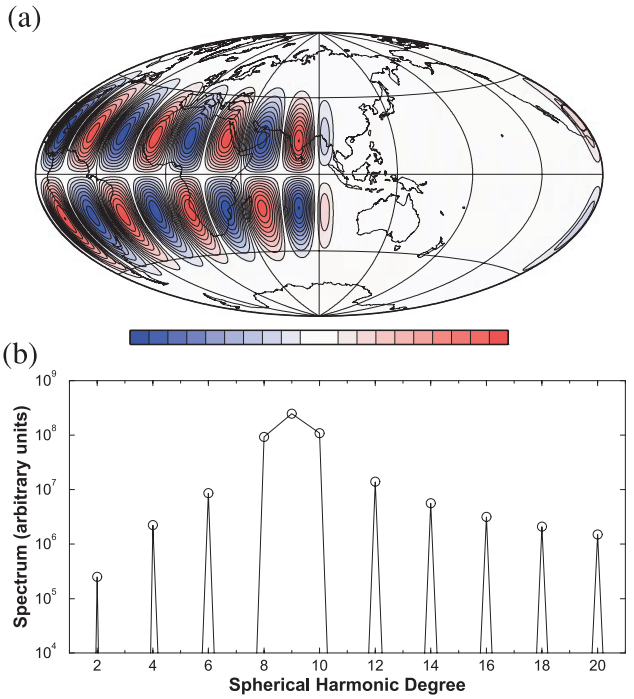

Figure 6. Synthetic test to demonstrate origin of the (small) dominance of power from even degree spherical harmonics in the power spectrum of Fig. 2. (a) Field for test. (b) Corresponding power spectrum.

Sabaka *et al.* (2004), and one epoch each from the C^{3}FM model of Wardinski & Holme (2006), and the gufm1 model of Jackson *et al.* (2000). All are compared against the model spectrum fit (eq. 11) calculated from CHAOS-4. The two precursors of CHAOS-4 show broadly the same spectral structure as this model, but with the departure from the trend line happening at lower harmonic degree (11 for CO2003). The GRIMM-2 model also follows this pattern, with the higher power at degree 13 suggesting that contamination from noise may be becoming significant. This is supported by mapping of GRIMM truncated to various degrees. Maps to degree 11 are indistinguishable from those in Fig. 4. At degree 13, the stronger features are common between the CHAOS-4 and GRIMM models, but noise in the map from the GRIMM model obscures possible low SV under Antarctica as seen from the CHAOS-4 model. Thus

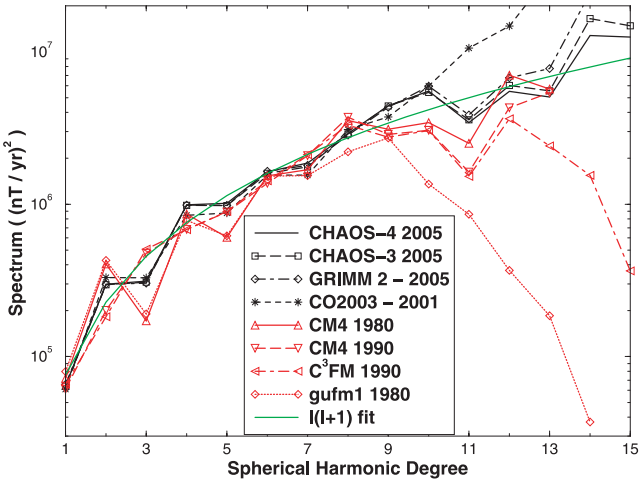

Figure 7. Spectra of a variety of model SV compared with that of CHAOS-4 at the CMB, $r = c$.

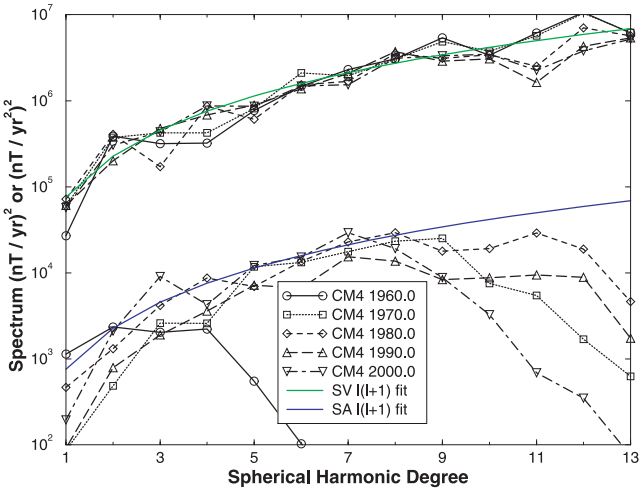

Figure 8. Spectra for CM4 in 10 yr intervals for SV (upper set of curves) and SA (lower set of curves). Reference curves from the fit for CHAOS-4 are also plotted.

our contention of low sub-Antarctic SV is as yet unconfirmed by another current model.

Of the models from earlier data, both C^{3}FM and gufm1 show the effects of damping, above spherical harmonic degrees 12 and 9, respectively. The highest power at high degrees (and so the best chance of higher-degree content for these earlier models) is seen for CM4. This is not surprising; CM4 is the most detailed and heavily parameterized of the models, and is likely to be of the highest resolution. CM4 models the geomagnetic field from 1960 to 2002.5; for most of this period, globally distributed vector data from satellites are not available, as prior to 1999 only one other satellite, Magsat, returned vector data, and that only for 6 months in 1980. Nonetheless, the detailed parameterization of external fields, and the length of the data series (1960–2002.5) optimize accurate modelling of SV. Spectra of the CM4 SV and SA from throughout the modelling period are presented in Fig. 8 at 10 yr intervals, along with the trend lines from the fit to the CHAOS-4 models. The SV spectra fit the reference curve well (possibly with slightly lower amplitude, which may be due to the damping of surface Laplacian of the SV during model construction). The SA is less well fit, as might be expected: the contributing data are less good than those for CHAOS-4, and in CM4 the SA is also damped, which would naturally depress these curves—this is seen particularly severely for the 1960.0 curve at the start of the modelling interval. Nevertheless, the curves clearly follow the trend curve, particularly for the later epochs where constraint from satellite data is stronger. Thus, the time constant of approximately 10 yrs calculated from eq. (14) is also supported by CM4, suggesting that this value reflects the physics of magnetic field generation rather than the length of available satellite data and the CHAOS-4 model.

Motivated by the similarity of the SV spectra to those from CHAOS-4, we plot the SV of CM4 at four epochs in Fig. 9, on the same scale and with the same colour scheme ignoring low SV magnitudes as for CHAOS-4 in Fig. 5. The low SV under the Pacific and North Atlantic is seen throughout, and under Antarctica is seen for 1990 and 2000. We cannot rule out that the stronger SV in 1980 and earlier is real, but prior to 1980, there are few data for this region, and therefore the SV may result from 'leakage' from better constrained regions (non-required SV under Antarctica allowing SV elsewhere to be expressed by lower-degree harmonics, which have a lower contribution to the global penalty norm), an

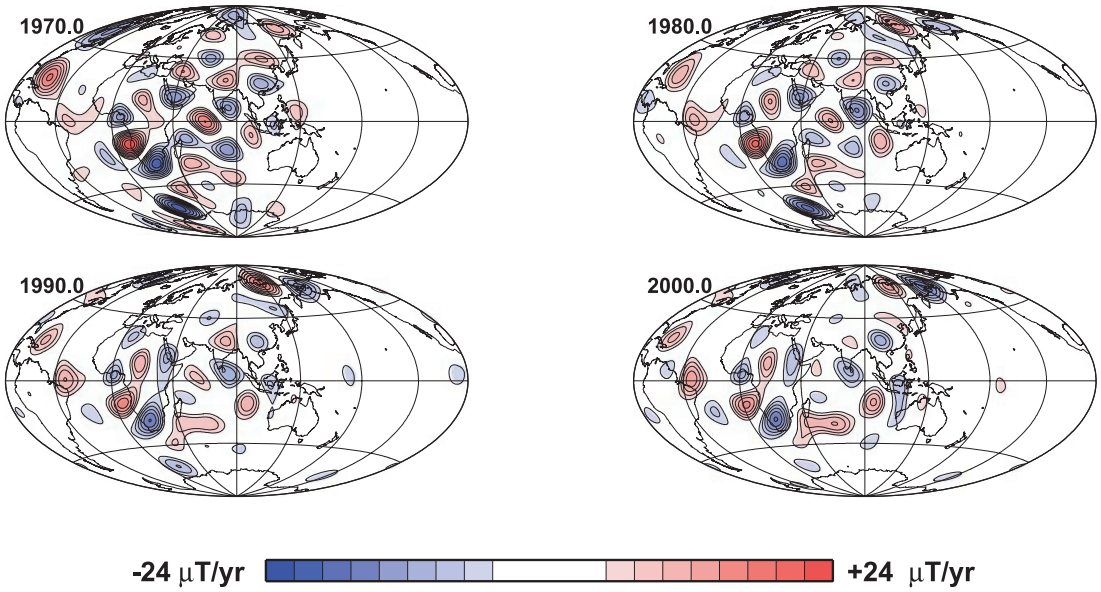

Figure 9. Radial component of the secular variation at the CMB, to maximum determined degree (13) for the model CM4. Compare with Fig. 5.

artefact of the regularization. To determine whether this is possible, it would be necessary to solve for the Comprehensive Model, but with additional 'data' of low (or zero) SV measurements at the CMB in regions of interest. Is it possible to find a model prior to 1980 that fits the data with these additional constraints? If so, then the low Antarctic SV may be longer lived as for the North Atlantic and Pacific.

5 GEOPHYSICAL INTERPRETATION

Perhaps the most thought-provoking result reported here is the uniform timescale for all scales of geomagnetic SV defined by eq. (14). The output from dynamo codes has been used to study time constants from the field and SV (e.g. Christensen & Tilgner 2004); it would be extremely interesting to extend that work to examine this new measure. It could be that the two timescales are measuring different processes, field/SV related to long-term evolution of core flow and SV/SA related to decadal variations. In this case, the dynamo codes might be expected not to match the relation obtained here, as they are generally not in the correct parameter regime to support short-timescale features of the SV.

When maps of the CMB field from Magsat were first obtained, these were not only interesting in their own right, but also served to give confidence to the interpretation of models from earlier, historical data. This work may be similar: the similarities between CHAOS-4 and CM4 suggest it is already possible to consider detailed SV over the past 30 yrs, and with care this may be extended back to a 50-yr window. It may even be possible to gain insight for earlier epochs, through analysis of the spectrum as in Fig. 6. For example, the SV spectrum for the model gufm1, epoch 1850, also shows values at low degree alternately above and below the trend, but with odd degrees dominant. This could arise from a similar SV structure as seen in the CHAOS-4 model, but with an odd number of SV flux patch pairs, rater than an even number as seen here.

The low SV in the Pacific hemisphere has been known for many years—this applies not only on historical timescales, but also on longer timescales, up to millions of years (the so-called Pacific dipole window). Various processes have been suggested to account for this, particularly thermal core–mantle coupling (Gubbins 2003) or electromagnetic screening due to highly conducting mantle under the Pacific. The suggestion for electromagnetic screening assumes that regions of anomalously low seismic shear wave velocity (the so-called Large Low Shear wave Velocity Province—LLSVP) also have anomalously high electrical conductivity. However, Fig. 5 reveals other regions of equally low SV, unrelated to seismic anomalies, and therefore with no grounds for assuming higher electrical conductivity. Thus maps presented here would favour instead thermal coupling having a large scale influence on the geodynamo, leading to localized areas of high SV, rather than localized low SV.

What direct interpretation can be made of the limited region of high SV? Considering these features in terms of difference in structure of core flow is attractive (perhaps arguing for localized strong flow under the Atlantic), but could be misleading. Gubbins & Kelly (1996) have argued that if the flow is broadly steady, as is suggested from core-flow modelling for the past 150 yrs, and arguably for the past 350 yrs (Whaler *et al.* 2011), then an equilibrium will be established between advection and diffusion, leading to no net SV. However, if SV is generated in a localized region, for example, by the expulsion of magnetic flux under Indonesia, such SV is not in advective/diffusive equilibrium, and so when carried along subsequently by the flow will be visible in the changing magnetic field structure, and act as a tracer for flow. That strong SV is seen localized under the Atlantic could therefore either be because flow is stronger there, or because a non-equilibrium source is well positioned for this flow to be revealed.

6 CONCLUSION

In this paper, we have demonstrated that geomagnetic models derived from data from low-Earth orbiting satellites are of sufficient resolution to successfully present maps of SV at the CMB. The spectrum of the SV at the CMB is 'blue'; nevertheless, coherent features are seen in maps to spherical harmonic degree 13. Many of these features are common to a model for earlier epochs, the Comprehensive Model CM4. Both SV and SA show a spectral form well fit by a function proportional to $l(l+1)$, where l is spherical harmonic degree; the ratio of the two spectra implies a 10-yr timescale for geomagnetic variation, independent of harmonic degree. It may

even be possible to get insight into (or at least constraint of) even earlier epochs by examination of details of the lower degree spectrum. We therefore propose that direct examination of SV is a fruitful potential tool in the future for constraining conditions and processes at the CMB.

ACKNOWLEDGMENTS

This study was supported under the NERC GEOSPACE consortium, NER/O/S/2003/00675. Flow plots were generated using GMT (Wessel & Smith 1998). We thank Vincent Lesur and an anonymous reviewer for comments that led to considerable clarification.

REFERENCES

Christensen, U. & Tilgner, A., 2004. Power requirement of the geodynamo from ohmic losses in numerical and laboratory dynamos, *Nature,* **429,** 169–171.

Gillet, N., Jackson, A. & Finlay, C.C., 2007. Maximum entropy regularization of time-dependent geomagnetic field models, *Geophys. J. Int.,* **171,** 1005–1016.

Gillet, N., Pais, M.A. & Jault, D., 2009. Ensemble inversion of time-dependent core flow models, *Geochem. Geophys. Geosys.,* **10,** Q06004, doi:10.1029/2008GC002290.

Gillet, N., Lesur, V. & Olsen, N., 2010. Geomagnetic core field secular variation, *Space Sci. Rev.,* **155,** 129–145.

Gubbins, D., 2003. Thermal core-mantle interactions: theory and observations, in *Earth's Core: Dynamics, Structure, Rotation,* Geodynamics Series Vol. 31, pp. 163–179, eds Dehant, V., Creager, K.C., Karato, S.-I. & Zatman, S., AGU, Washington, DC.

Gubbins, D. & Kelly, P., 1996. A difficulty with using the frozen flux hypothesis to find steady core motions, *Geophys. Res. Lett.,* **23,** 1825–1828.

Holme, R. & Olsen, N., 2006. Core surface flow modelling from high-resolution secular variation, *Geophys. J. Int.,* **166,** 518–528.

Hulot, G. & Le Mouël, J.L., 1994. A statistical approach to the Earth's main magnetic field, *Phys. Earth planet. Int.,* **82,** 167–183.

Hulot, G., Eymin, C., Langlais, B., Mandea, M. & Olsen, N., 2002. Small-scale structure of the geodynamo inferred from Oersted and MAGSAT satellite data, *Nature,* **416,** 620–623.

Jackson, A., 2003. Intense equatorial flux splots on the surface of the Earth's core, *Nature,* **424,** 760–763.

Jackson, A., Jonkers, A.R.T. & Walker, M.R., 2000. Four centuries of geomagnetic secular variation from historical records, *Philos. Trans. R. Soc. Lond. A,* **358,** 957–990.

Langel, R.A. & Estes, R.H., 1982. A geomagnetic field spectrum, *Geophys. Res. Lett.,* **9,** 250–253.

Lesur, V., Wardinski, I., Rother, M. & Mandea, M., 2008. GRIMM: the GFZ reference internal magnetic model based on vector satellite and observatory data, *Geophys. J. Int.,* **173,** 382–394.

Lesur, V., Wardinski, I., Hamoudi, M. & Rother, M., 2010. The second generation of the GFZ reference internal magnetic model: GRIMM-2, *Earth Planets Space,* **62,** 765–773.

Lhuillier, F., Fournier, A., Hulot, G. & Aubert, J., 2011. The geomagnetic secular-variation timescale in observations and numerical dynamo models, *Geophys. Res. Lett.,* **38,** L09306, doi:10.1029/2011GL047356.

Lowes, F.J., 1966. Mean-square values on sphere of spherical harmonic vector fields, *J. geophys. Res.,* **71,** 8, doi:10.1029/jZ071i008p02179.

Lowes, F.J., 1974. Spatial power spectrum of the main geomagnetic field, and extrapolation to the core, *Geophys. J. R. astron. Soc.,* **36,** 717–730.

Mandea, M., Holme, R., Pais, A., Pinheiro, K., Jackson, A. & Verbanac, G., 2010. Geomagnetic jerks: rapid core field variations and core dynamics, *Space Sci. Rev.,* **155,** 147–175.

Mauersberger, P., 1956. Das Mittel der Energiedichte des geomagnetischen Hauptfeldes an der Erd-oberfläche und seine säkulare Änderung, *Gerlands Beitr. Geophys.,* **65,** 207–215.

Maus, S., Rother, M., Stolle, C., Mai, W., Choi, S., Lühr, H., Cooke, D. & Roth, C., 2006. Third generation of the Potsdam magnetic model of the Earth (POMME), *Geochem. Geophys. Geosyst,* **7,** Q07008, doi:10.1029/2006GC001269.

McLeod, M.G., 1996. Spatial and temporal power spectra of the geomagnetic field, *J. geophys. Res.,* **101,** 2745–2763.

Neubert, T. et al., 2001. Ørsted satellite captures high-precision geomagnetic field data, *EOS, Trans. Am. geophys. Un.,* **82,** 81–88.

Olsen, N., Lühr, H., Sabaka, T.J., Mandea, M., Rother, M., Tøffner-Clausen, L. & Choi, S., 2006. CHAOS – a model of the Earth's magnetic field derived from CHAMP, Ørsted, and SAC-C magnetic satellite data, *Geophys. J. Int.,* **166,** 67–75.

Olsen, N., Mandea, M., Sabaka, T.J. & Tøffner-Clausen, L., 2009. CHAOS-2 – a geomagnetic field model derived from one decade of continuous satellite data, *Geophys. J. Int.,* **179,** 1477–1487.

Olsen, N., Lühr, H., Sabaka, T.J., Michaelis, I., Rauberg, J. & Tøffner-Clausen, L., 2010a. *A high-resolution geomagnetic field model derived from low-altitude CHAMP data*. Abstract GP21A-0992, 2010 Fall Meeting, AGU, San Francisco, CA.

Olsen, N., Mandea, M., Sabaka, T.J. & Tøffner-Clausen, L., 2010b. The CHAOS-3 geomagnetic field model and candidates for the 11th generation IGRF, *Earth Planets Space,* **62,** 719–727.

Reigber, C., Lühr, H. & Schwintzer, P., 2002. CHAMP mission status, *Adv. Space Res.,* **30,** 129–134.

Sabaka, T.J., Olsen, N. & Langel, R.A., 2004. Extending comprehensive models of the Earth's magnetic field with ørsted and CHAMP data, *Geophys. J. Int.,* **159,** 521–547.

Stacey, F.D., 1992. *Physics of the Earth,* Brookfield, Brisbane.

Voorhies, C.V., 1998. *Elementary theoretical forms for the spatial magnetic power spectrum of Earth's crustal magnetic field*. NASA Tech. pap., 1998-208608, 38 pp.

Voorhies, C.V., 2004. Narrow scale flow and a weak field by the top of Earth's core: evidence from Ørsted, MAGSAT and secular variation, *J. geophys. Res.,* **109,** B03106, doi:10.1029/2003JB002833.

Voorhies, C.V., Sabaka, T.J. & Purucker, M., 2002. On magnetic spectra of Earth and Mars, *J. geophys. Res.,* **107,** E6, doi:10.1029/2001JE001534.

Wardinski, I. & Holme, R., 2006. A time-dependent model of the Earth's magnetic field and its secular variation for the period 1980–2000, *J. geophys. Res.,* **111,** B12101, doi:10.1029/2006JB004401.

Wessel, P. & Smith, W.H.F., 1998. New, improved version of the generic mapping tools released, *EOS, Trans. Am. geophys. Un.,* **79,** 579.

Whaler, K.A., Holme, R. & Lynch, C.A., 2011. The axial dipole strength and flow in the outer core, *Phys. Earth planet. Inter.,* in press.